J|A|C|S

JOURNAL OF THE AMERICAN CHEMICAL SOCIETY
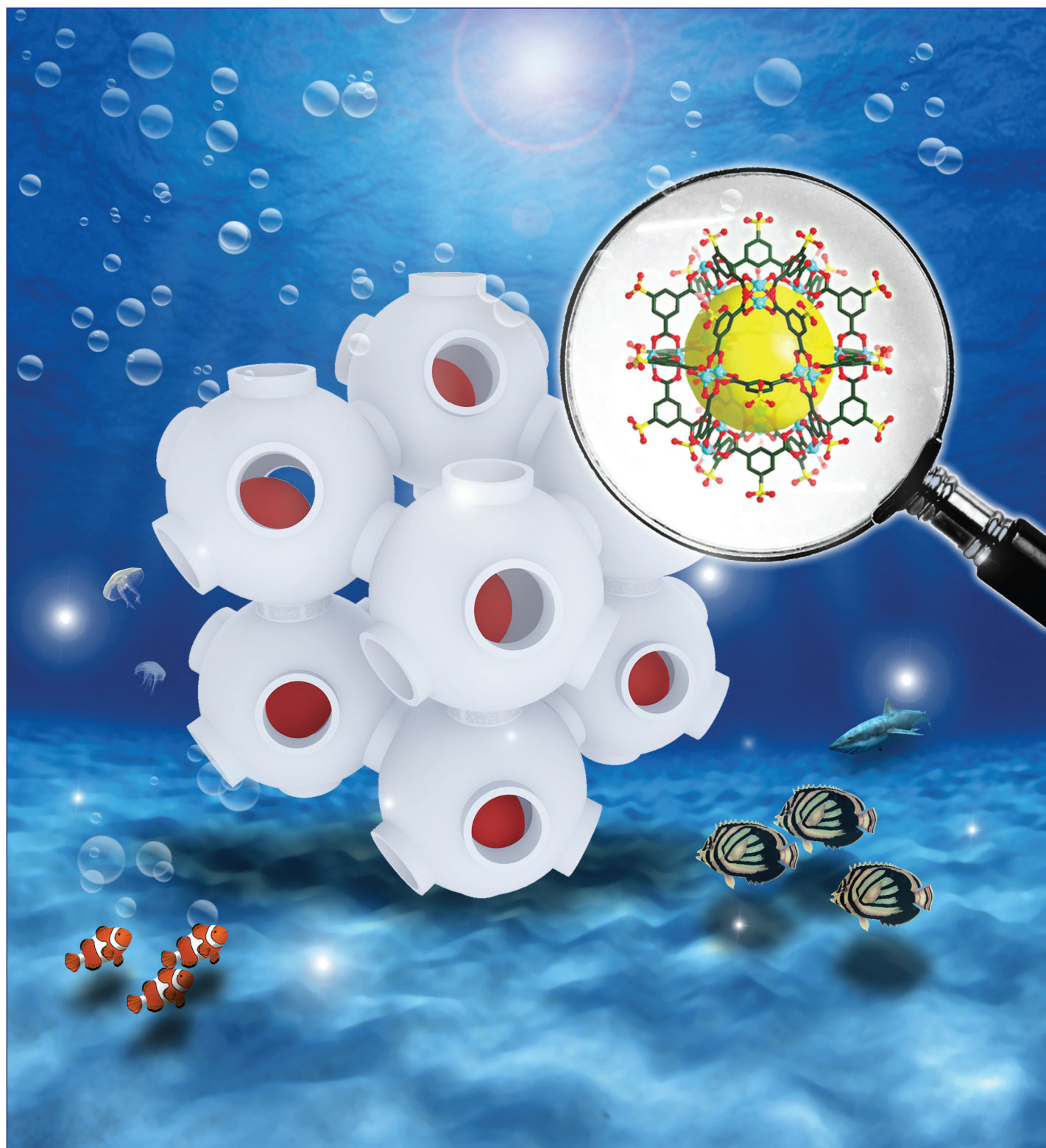
Single Atom (Pd/Pt) Supported on Graphitic Carbon Nitride as an Efficient Photocatalyst for Visible-Light Reduction of Carbon Dioxide

Guoping Gao,[†] Yan Jiao,[‡] Eric R. Waclawik,[†] and Aijun Du*,[†]

[†]School of Chemistry, Physics and Mechanical Engineering, Queensland University of Technology, Garden Point Campus, Brisbane, QLD 4001, Australia

[‡]School of Chemical Engineering, University of Adelaide, Adelaide, SA 5005, Australia

S Supporting Information

ABSTRACT: Reducing carbon dioxide to hydrocarbon fuel with solar energy is significant for high-density solar energy storage and carbon balance. In this work, single atoms of palladium and platinum supported on graphitic carbon nitride (g-C_3N_4), i.e., Pd/g-C_3N_4 and Pt/g-C_3N_4, respectively, acting as photocatalysts for CO_2 reduction were investigated by density functional theory calculations for the first time. During CO_2 reduction, the individual metal atoms function as the active sites, while g-C_3N_4 provides the source of hydrogen (H*) from the hydrogen evolution reaction. The complete, as-designed photocatalysts exhibit excellent activity in CO_2 reduction. HCOOH is the preferred product of CO_2 reduction on the Pd/g-C_3N_4 catalyst with a rate-determining barrier of 0.66 eV, while the Pt/g-C_3N_4 catalyst prefers to reduce CO_2 to CH_4 with a rate-determining barrier of 1.16 eV. In addition, deposition of atom catalysts on g-C_3N_4 significantly enhances the visible-light absorption, rendering them ideal for visible-light reduction of CO_2. Our findings open a new avenue of CO_2 reduction for renewable energy supply.
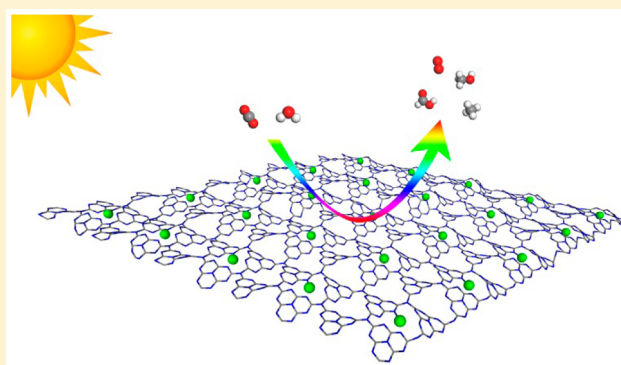
1. INTRODUCTION

Because of the continuing increase in the emissions of CO_2 from human activities, the reduction of CO_2 into alternative fuels such as formic acid (HCOOH), methanol (CH_3OH), and methane (CH_4) is a critical goal that would positively impact the global carbon balance and energy storage.[1-3] As CO_2 is an extremely stable and unreactive molecule, the conversion of CO_2 to fuels is a scientifically challenging problem that requires appropriate catalysts and high energy input.[1] The current industrial process for reducing CO_2 to methanol using H_2 is carried out at high temperature (496−573 K) and high pressure (5−10 MPa) using Cu-ZnO/Al_2O_3 as a catalyst.[4] Tremendous efforts in both academic research and industry have been devoted to developing efficient catalysts for CO_2 reduction at a low energy cost.[5-9]

The deposition of metal nanoclusters on substrates as heterogeneous catalysts has been widely used in many important reactions.[10-12] The ultimate small-size limit for metal clusters is a single atom, in which isolated metal atoms are dispersed on a substrate.[13] Using only single or a few metal atoms as active sites, such nanostructured catalysts not only minimize materials usage but also exhibit fascinating activity due to their high ratio of low-coordinated metal atoms, which usually function as active sites.[14,15] However, isolating nanostructured clusters still remains a significant experimental challenge because the surface free energy of clusters increases

as the size of the particles decreases.[16] An appropriate substrate that strongly interacts with the clusters is required in order to prevent their aggregation. Metal oxides strongly interact with single-atom/cluster metal catalysts through surface oxygen[17-20] and have been widely used as substrates to isolate single metal atoms or clusters efficiently. In recent experiments, cluster catalysts with precise numbers of atoms, such as Cu_4 and Ag_3 clusters supported by Al_2O_3, have shown high catalytic activity toward particular reactions in both experiments and theoretical calculations.[17-19,21] Furthermore, the experimental realization of single-atom catalysts on metal oxide substrates, including Pt_1/FeO_x,[21] Ag_1/MgO,[22] and Ru_1/Co_3O_4,[23] presages the use of these precious-metal catalysts economically. However, the oxygens of the metal oxide substrates actually partially oxidize the single atom/cluster catalyst and so diminishes the activity.[18,24-26]

Graphitic carbon nitride (g-C_3N_4) is a promising stable, active, metal-free photocatalyst capable of efficiently splitting water into hydrogen.[27-29] It has also been reported to be an excellent substrate for supporting catalysts.[30] Using g-C_3N_4 as a substrate to support noble-metal catalysts for CO_2 hydrogenation offers a number of inherent advantages, including maintaining the noble-metal atoms in their neutral state,

directly providing the hydrogen source, and possessing excellent solar light absorption.[31,32] A recent advance in the use of g-C_3N_4 as a catalyst substrate made by Vilé and colleagues,[33] who showed that isolated Pd atoms could be tenaciously attached to the pyridinic nitrogen atoms of g-C_3N_4. Meanwhile, single Pt atoms supported on g-C_3N_4 were synthesized in a recent experiment that exhibited excellent photocatalytic hydrogen evolution activity.[34] In this work, the newly realized single-atom catalysts supported on g-C_3N_4, including Pd/g-C_3N_4 and Pt/g-C_3N_4, were investigated for the first time for the reduction of CO_2 into hydrocarbon fuels by means of density functional theory (DFT) calculations. The differential charge density demonstrated that Pd and Pt atoms form strong interactions with g-C_3N_4 by exchanging electron density, with less net electron transfer from Pd and Pt to g-C_3N_4 than to FeO_x,[19] which is good for activation of the Lewis acid CO_2. The reaction pathways for CO_2 reduction on single-atom catalysts (Pd and Pt) supported on g-C_3N_4 were obtained by the climbing image nudged elastic band (CI-NEB) method. As evaluated by the reaction barriers, the preferred product of CO_2 reduction on the Pd/g-C_3N_4 catalyst is HCOOH with a barrier of 0.66 eV, while the Pt/g-C_3N_4 catalyst is able to reduce CO_2 to CH_4 efficiently with a barrier of 1.16 eV, which is smaller than that reported in ref 18. Interestingly, the optical absorption spectra demonstrate that Pt and Pd supported on g-C_3N_4 extend the absorption edge of g-C_3N_4 from 2.7 to 0.2 eV, leading to significant enhancement of the visible-light absorption efficiency.

2. COMPUTATIONAL METHODS

DFT calculations were performed by using the Vienna Ab Initio Simulation Package (VASP).[35,36] The exchange−correlation interactions were treated within the generalized gradient approximation (GGA)[37] in the form of the Perdew−Burke−Ernzerhof (PBE) functional.[38] The van der Waals interactions were described using the empirical correction in Grimme's scheme (i.e., DFT+D3).[39] The electron wave functions were expanded using plane waves with a cutoff energy of 500 eV, and the convergence criteria for the residual force and energy on each atom during structure relaxation were set to 0.005 eV/Å and 10^{-5} eV, respectively. The vacuum space was more than 20 Å, which was enough to avoid interactions between periodic images. The CI-NEB method was used to find saddle points and minimum-energy paths.[40] The single-atom catalysts were modeled by depositing one metal atom on 2 × 2 × 1 supercell g-C_3N_4. The Brillouin zone (BZ) was sampled with a Monkhorst−Pack mesh with a 3 × 3 × 1 k-point grid in reciprocal space during geometry optimization and NEB calculations.

Hybrid functionals based on the Heyd−Scuseria−Ernzerhof (HSE06) method[41,42] were adopted to get the exact band structures and optical absorption spectra of the Pd/g-C_3N_4 and Pt/g-C_3N_4 catalysts, with a 5 × 5 × 1 k-point grid in reciprocal space. VASP was used to calculate the frequency-dependent dielectric function after the electronic ground state was determined. The imaginary part of the dielectric function is determined by a summation over empty states using eq 1:[43]

$$\varepsilon_{\alpha\beta}^{(2)}(\omega) = \frac{4\pi^2 e^2}{\Omega} \lim_{q\to 0} \frac{1}{q^2} \sum_{c,v,k} 2\omega_k \delta(\epsilon_{ck} - \epsilon_{vk} - \omega)|\langle u_{ck+q}|u_{vk}\rangle|^2$$

(1)

where the indices c and v refer to conduction and valence band states, respectively.

3. RESULTS AND DISCUSSION

To find the most favorable deposition sites for the single-atom catalysts, various positions on the 2 × 2 × 1 g-C_3N_4 supercell

were considered, as shown in Figure 1a and Table S1 in the Supporting Information. The optimized structures and the 3D
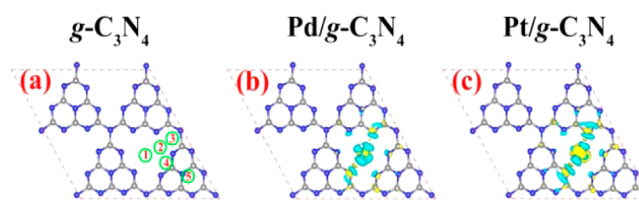
**Figure 1.** (a) Optimized structure of pristine g-C_3N_4. Positions: 1, center of the sixfold cavity; 2, corner of the sixfold cavity; 3, top of the five-membered ring; 4, edge of the sixfold cavity; 5, top of g-C_3N_4. (b, c) Plots of 3D differential charge densities of (b) Pd/g-C_3N_4 and (c) Pt/g-C_3N_4 at isosurfaces of −0.005 e/Å³ (yellow, charge accumulation) and 0.005 e/Å³ (blue, charge depletion).

differential charge densities of Pd/g-C_3N_4 and Pt/g-C_3N_4 are plotted in Figure 1b,c. The sixfold cavity of g-C_3N_4 is the most stable site for the deposition of Pd and Pt atoms, and the calculated binding energies are −2.17 and −2.95 eV respectively. These results are collectively consistent with those reported in ref 33. It can be clearly seen from the differential charge densities (Figure 1b,c) that there is significant charge transfer between the metal atoms and the neighboring pyridinic nitrogen atoms for both Pd/g-C_3N_4 and Pt/g-C_3N_4, indicating a strong interaction between the lone-pair electrons of the neighboring pyridinic nitrogen atoms and the isolated metal atoms. The charge is mainly depleted in the d orbitals of Pd/g-C_3N_4, while both charge accumulation and depletion occur around the Pt atom in Pt/g-C_3N_4. Consequently, the valence (oxidation) states of Pd and Pt on g-C_3N_4 are only +0.40 and +0.27, respectively, on the basis of Bader charge analysis; these are lower than the values of +0.61 for Pd[19] and +0.45 for Pt[21] supported on Fe_2O_3. Transition metal catalysts in a lower oxidation state generally possess stronger ability to capture the adsorbate and thus have higher catalytic activity.[18] Therefore, single Pd and Pt atoms supported on g-C_3N_4 are expected to be more active catalysts than Pd and Pt atoms supported on metal oxide substrates. The metal atoms will move to a corner of the sixfold cavity in g-C_3N_4 once reactant/intermediates (discussed in the following) are adsorbed on it during the reaction.

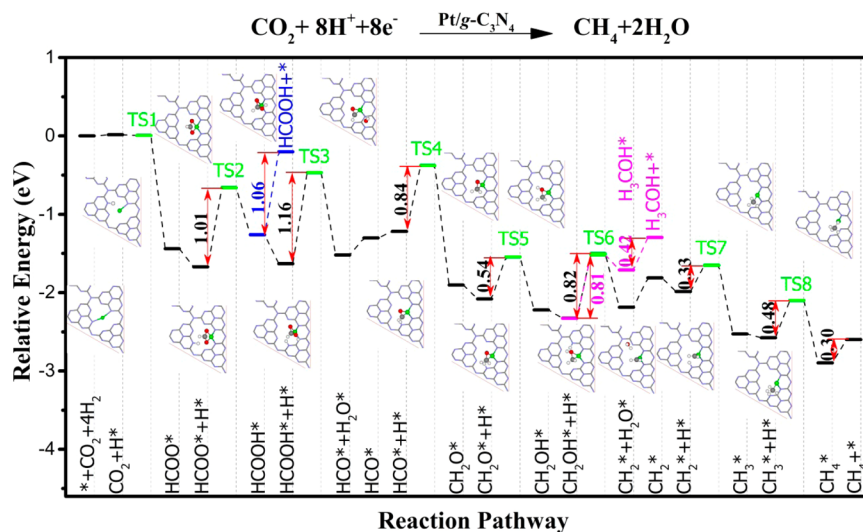The CO_2 reduction pathways to HCOOH and CH_3OH on the Pd/g-C_3N_4 catalyst were studied in detail, as shown in Figure 2. The overall reaction of CO_2 reduction to form CH_3OH on the Pd/g-C_3N_4 catalyst in the presence of hydrogen is expressed as follows:

$$CO_2 + 6H^+ + 6e^- \rightarrow CH_3OH + H_2O$$

(2)
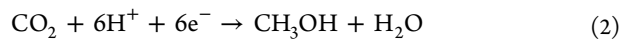
Although the pyridinic N atoms demonstrate high catalytic activity in hydrogen evolution, they are inert to the CO_2 reduction reaction. Herein, the Pd acts as the active site for the formation of carbon intermediates while the g-C_3N_4 provides the hydrogen source from the hydrogen evolution reaction ($H^+ + e^- \rightarrow H^*$) for the hydrogenation of CO_2[27,28] during CO_2 reduction. The reaction includes six elemental hydrogenation steps, which are determined by the most stable product at each step. The initial step of CO_2 reduction is the formation of HCOO*, which is followed by the hydrogenation of HCOO* to give HCOOH*. The approach of a third hydrogen induces the dissociation of HCOOH into HCO* and H_2O^*. The HCO* is further hydrogenated to form CH_2O^*,
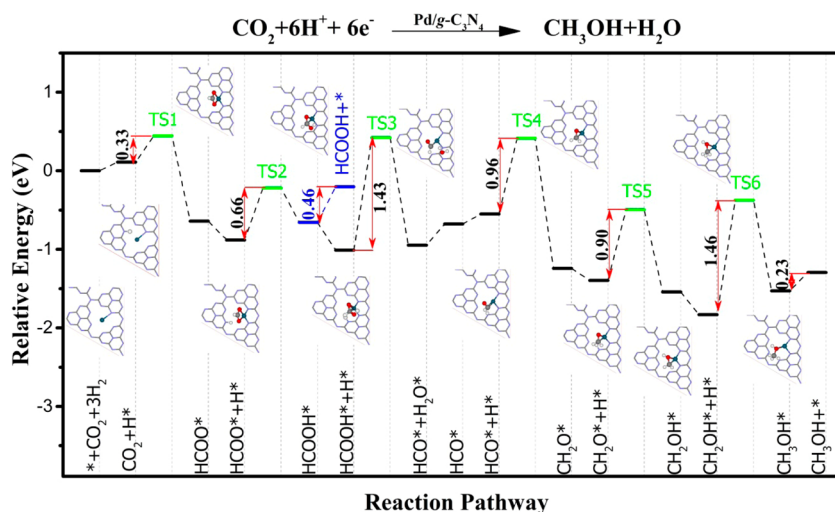
Figure 2. Reaction pathways for CO_2 reduction to HCOOH and CH_3OH on the Pd/g-C_3N_4 catalyst. Under standard conditions (pH 0, $p(H_2) = 1$ bar, $U = 0$ V vs SHE), the total energies of $H^+(aq) + e^-$ and $\frac{1}{2}H_2(g)$ are equal. The reference energy (the total free energy of the catalyst, isolated CO_2 and three H_2) is set to zero. The important intermediates and products are shown as well. The substrate is displayed partly in stick model. Color code for the catalyst and small molecules: Pt, green; C, gray; O, red; H, white.

Figure 3. Reaction pathways for CO_2 reduction to COOH, CH_3OH, and CH_4 on the Pt/g-C_3N_4 catalyst. Under standard conditions (pH 0, $p(H_2) = 1$ bar, $U = 0$ V vs SHE), the total energies of $H^+(aq) + e^-$ and $\frac{1}{2}H_2(g)$ are equal. The reference energy (the total free energy of the catalyst, isolated CO_2, and four H_2) is set to zero. The important intermediates and products are shown as well. The substrate is displayed partly in stick model. Color code: Pd, pine green; C, gray; O, red; H, white.

CH_2OH^*, and the final product, CH_3OH^*. All of the intermediates and products are adsorbed on the Pd atom, reacting with the hydrogen (H^*) that is bonded to the g-C_3N_4. The rate-determining step of the CH_3OH generation pathway on the Pd/g-C_3N_4 catalyst is the hydrogenation of CH_2OH^*, with a barrier of 1.46 eV. The second largest barrier is around 1.43 eV for the formation of HCO*. It should be noted that these barriers are lower than that on the Cu(111) surface (1.60 eV) and comparable to that on the Cu_{29} cluster (1.41 eV).[5] Therefore, the Pd/g-C_3N_4 catalyst possesses an excellent catalytic activity for CO_2 reduction.

The formation of HCOOH,

$$CO_2 + 2H^+ + 2e^- \rightarrow HCOOH \qquad (3)$$

follows the first two steps of the CH_3OH pathway, after which the HCOOH* desorbs directly from the Pd/g-C_3N_4 catalyst.

The rate-determining step of the HCOOH pathway is the second step, with a barrier of 0.66 eV, which is 0.80 eV lower than the rate-determining barrier for the formation of CH_3OH (1.46 eV). In addition, HCOOH is able to desorb from the Pd/g-C_3N_4 catalyst easily with a desorption energy of 0.46 eV. Therefore, the preferred product for CO_2 reduction on the Pd/g-C_3N_4 catalyst is the HCOOH pathway rather than the CH_3OH pathway.

In general, the stronger the adsorption of the intermediates on the catalyst is,[17,18] the lower is the barrier for a chemical reaction that can be obtained. Pt is expected to have much stronger interactions with hydrocarbon reactants than Pd because of its two uncoupled electrons. In Figure 3 we present the minimum energy pathways for CO_2 reduction to HCOOH, CH_3OH, and CH_4 on the Pt/g-C_3N_4 catalyst. The pathways for the formation of HCOOH and CH_3OH on the Pt/g-C_3N_4

catalyst are found to be nearly the same as those on the Pd/g-C_3N_4 catalyst but are thermodynamically more favorable because of the stronger interactions between Pt and the reaction intermediates. It can be clearly seen from Figure 3 that the strong interactions have a significant impact on the pathway for HCOOH production on the Pt/g-C_3N_4 catalyst. The barrier for the hydrogenation of HCOO* on the Pt/g-C_3N_4 catalyst (1.01 eV) is much higher than that on the Pd/g-C_3N_4 catalyst (0.66 eV), and the desorption of HCOOH from the Pt/g-C_3N_4 catalyst possesses the largest barrier on the entire reaction pathway (1.06 eV), while the desorption energy from the Pd/g-C_3N_4 catalyst is only 0.46 eV, suggesting that the formation of HCOOH is unfavorable for CO_2 reduction on the Pt/g-C_3N_4 catalyst. However, once the HCOOH* is formed, the following steps, including the dissociation of HCOOH* to form HCO* and the hydrogenation of HCO* to afford CH_2O*, CH_2OH*, and CH_3OH* during the formation of CH_3OH on the Pt/g-C_3N_4 catalyst become more favorable than those on the Pd/g-C_3N_4 catalyst (see Figure 2). The barriers for all of the reaction steps are much lower than those on the Pd/g-C_3N_4 catalyst. The third step, i.e., the hydrogenation of HCOOH on the Pt/g-C_3N_4 catalyst, is the rate-determining step, with a barrier of 1.16 eV. The largest barrier for the formation of CH_3OH on the Pt/g-C_3N_4 catalyst is lower than those on the Pd/g-C_3N_4 catalyst (1.46 eV), the Cu_{29} cluster (1.41 eV), Cu(111) (1.60 eV),[5] and Cu_4/Al_2O_3 (1.21 eV).[18]

We also studied the reaction pathway for the reduction of CO_2 into CH_4 on the Pt/g-C_3N_4 catalyst, as shown in eq 4:

$$CO_2 + 8H^+ + 8e^- \rightarrow CH_4 + 2H_2O \qquad (4)$$
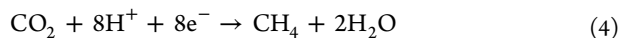
The few first reaction steps follow the same pathway as in the formation of CH_3OH up to the formation of CH_2OH*. Then the OH dissociates from CH_2OH* and bonds with hydrogen to form CH_2* and H_2O*. The barrier for dissociation of OH from CH_2OH* during the formation of CH_4 (0.82 eV) is comparable to that for the hydrogenation of CH_2OH* during the formation of CH_3OH (0.81 eV). However, CH_2* + H_2O* is more stable than CH_2OH* by 0.47 eV in total energy, indicating that the formation of CH_4 is highly feasible. Then the CH_2* is further hydrogenated to CH_3* and CH_4* with barriers of 0.38 and 0.48 eV, respectively. The rate-determining step for the formation of CH_4 is the hydrogenation of HCOOH, with a barrier of 1.16 eV, which is the same as that for the formation of CH_3OH on the Pt/g-C_3N_4 catalyst. It should be noted that such a barrier is much lower than that on Cu_4 (1.69 eV).[18] Since the CH_4 product is more thermodynamically stable than CH_3OH, the formation of CH_4 is likely to be the most dominant reaction pathway on the Pt/g-C_3N_4 catalyst. For comparison, we also investigated the pathway for the reduction of CO_2 on the Cu/g-C_3N_4 catalyst. We found that the interactions between Cu/g-C_3N_4 and the reactant/intermediates are weak. For instance, the adsorption energies of HCOOH on the Pd/g-C_3N_4 and Pt/g-C_3N_4 catalysts are −0.46 and −1.06 eV, respectively, while that on the Cu/g-C_3N_4 catalyst is only −0.35 eV. The weak interactions between Cu/g-C_3N_4 and the reaction intermediates lead to a large barrier for the formation of CH_3OH on the Cu/g-C_3N_4 catalyst (1.79 eV). This suggests that the Cu/g-C_3N_4 catalyst is not promising for CO_2 reduction (more details can be found in Figure S1 in the Supporting Information).

Previous work has demonstrated that pure g-C_3N_4 can be a potential photocatalyst for hydrogen production[29] and the reduction of CO_2.[44] However, g-C_3N_4 shows only minimal

visible-light absorption because it has a relatively large band gap (2.7 eV).[45] The deposition of isolated Pt and Pd atoms on g-C_3N_4 is expected to significantly modify its electronic structure and might enhance the visible-light response. Figure 4 presents
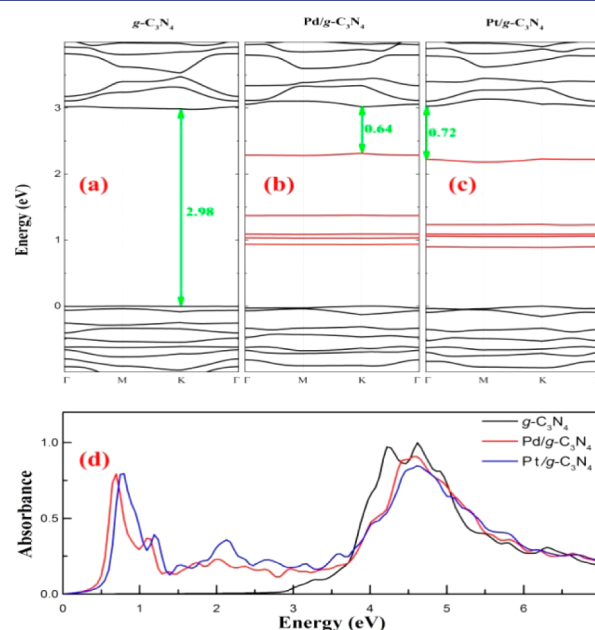
Figure 4. (a−c) Band structures and (d) optical absorption spectra of g-C_3N_4, Pd/g-C_3N_4, and Pt/g-C_3N_4. For the purpose of comparison, the contributions of the metal atom in the band structures are distinguished by red coloring, and the top of the valence states in pristine g-C_3N_4, Pd/g-C_3N_4, and Pt/g-C_3N_4 have been shifted to zero.

the calculated band structures (a−c) and optical absorption spectra (d) of pristine g-C_3N_4, Pd/g-C_3N_4, and Pt/g-C_3N_4 using a state-of-the-art hybrid functional. The band gap of g-C_3N_4 was calculated to be 2.98 eV, which is in good agreement with the experimental value.[45] With Pd/Pt atoms deposited on the g-C_3N_4, we found that the occupied d bands of the metal atoms lie in the gap of the band structure of g-C_3N_4. Consequently, the band gaps of Pd/g-C_3N_4 and Pt/g-C_3N_4 are significantly reduced to 0.64 and 0.72 eV, respectively. In addition, the conduction-band minima for Pd/g-C_3N_4 and Pt/g-C_3N_4 are located around −0.91 and −0.90 V, respectively, with respect to the normal hydrogen electrode (NHE), which are more negative than the standard electrode potentials of CO_2/HCOOH (−0.61 V vs NHE), CO_2/CH_3OH (−0.38 V vs NHE), and CO_2/CH_4 (−0.24 V vs NHE).[46] As the valence-band maxima of Pd/g-C_3N_4 (−0.27 V vs NHE) and Pt/g-C_3N_4 (−0.18 V vs NHE) are located above the potential for the production of O_2 (1.23 V vs NHE), a proper sacrificial electron donor may be required to promote the hydrogen evolution reaction.[32]

Most interestingly, the narrower gaps of Pd/g-C_3N_4 and Pt/g-C_3N_4 compared with pristine g-C_3N_4 lead to a red shift of the optical absorption spectra and thus enhance the visible-light harvesting, as shown in Figure 4d. As can be seen, the main light absorption peak of pure g-C_3N_4 is located at around 4.5 eV, and the absorption edge ends at 2.7 eV. With a Pd or Pt atom deposited on g-C_3N_4, a new absorption peak appears at 0.7 eV and the absorption edge extends to 0.2 eV, which could be ascribed to the electron excitation from the d band of the metal atom to the conduction band of g-C_3N_4. Therefore,

single atom (Pd/Pt) supported on g-C_3N_4 is also able to harvest visible and infrared light with a higher solar conversion efficiency compared with the pure g-C_3N_4 material. In the presence of a proper sacrificial electron donor,[32] the photogenerated electrons will be transferred to the conduction band of g-C_3N_4 and participate in proton reduction to provide the hydrogen source (H*) for CO_2 reduction. Therefore, the reaction pathways shown in Figures 2 and 3 may be better promoted by visible light.

4. CONCLUSIONS

Single metal atoms, including Pd and Pt, supported on g-C_3N_4 as photocatalysts for CO_2 reduction by hydrogen were investigated by DFT calculations. During the reaction, the noble atom functions as the active site while the g-C_3N_4 provides the hydrogen source from the hydrogen evolution reaction. A single-atom catalyst not only can maximize the efficiency of noble-metal atoms but also exhibits excellent activity for CO_2 reduction. As evaluated by the reaction barriers, the preferred product of CO_2 reduction on the Pd/g-C_3N_4 catalyst is HCOOH with a barrier of 0.66 eV, while the Pt/g-C_3N_4 catalyst is able to reduce CO_2 to CH_4 efficiently with a barrier of 1.16 eV. In addition, the single metal atoms supported on g-C_3N_4 significantly enhance the visible-light absorption, making these materials potential photocatalysts for visible-light-promoted reduction of CO_2. Our results provide a new clue for experimental validation to convert CO_2 into fuel using solar energy.

■ ASSOCIATED CONTENT

ⓢ Supporting Information

The Supporting Information is available free of charge on the ACS Publications website at DOI: 10.1021/jacs.6b02692.

> Binding energies of Pt and Pd on g-C_3N_4 at different adsorption sites shown in Table S1, elemental steps for the formation of HCOOH, CH_3OH, and CH_4, and reaction pathways for CO_2 reduction to HCOOH and CH_3OH on the Cu/g-C_3N_4 catalyst (Figure S1) (PDF)

■ AUTHOR INFORMATION

Corresponding Author

*aijun.du@qut.edu.au

Notes

The authors declare no competing financial interest.

■ ACKNOWLEDGMENTS

■ REFERENCES

(1) Benson, E. E.; Kubiak, C. P.; Sathrum, A. J.; Smieja, J. M. *Chem. Soc. Rev.* **2009**, *38*, 89.
(2) Li, C. W.; Ciston, J.; Kanan, M. W. *Nature* **2014**, *508*, 504.
(3) Li, F.-F.; Lau, J.; Licht, S. *Adv. Sci.* **2015**, *2*, 1500260.
(4) Waugh, K. C. *Catal. Today* **1992**, *15*, 51.
(5) Yang, Y.; Evans, J.; Rodriguez, J. A.; White, M. G.; Liu, P. *Phys. Chem. Chem. Phys.* **2010**, *12*, 9909.
(6) Kim, Y.; Trung, T. S. B.; Yang, S.; Kim, S.; Lee, H. *ACS Catal.* **2016**, *6*, 1037.
(7) Sampson, M. D.; Kubiak, C. P. *J. Am. Chem. Soc.* **2016**, *138*, 1386.
(8) Kornienko, N.; Zhao, Y.; Kley, C. S.; Zhu, C.; Kim, D.; Lin, S.; Chang, C. J.; Yaghi, O. M.; Yang, P. *J. Am. Chem. Soc.* **2015**, *137*, 14129.
(9) Gao, D.; Zhou, H.; Wang, J.; Miao, S.; Yang, F.; Wang, G.; Wang, J.; Bao, X. *J. Am. Chem. Soc.* **2015**, *137*, 4288.
(10) Tyo, E. C.; Vajda, S. *Nat. Nanotechnol.* **2015**, *10*, 577.
(11) Xie, L.; Brault, P.; Coutanceau, C.; Bauchire, J.-M.; Caillard, A.; Baranton, S.; Berndt, J.; Neyts, E. C. *Appl. Catal., B* **2015**, *162*, 21.
(12) Wu, Q.; Xiong, S.; Shen, P.; Zhao, S.; Li, Y.; Su, D.; Orlov, A. *Catal. Sci. Technol.* **2015**, *5*, 2059.
(13) Yan, H.; Cheng, H.; Yi, H.; Lin, Y.; Yao, T.; Wang, C.; Li, J.; Wei, S.; Lu, J. *J. Am. Chem. Soc.* **2015**, *137*, 10484.
(14) Gao, G.-P.; Wei, S.-H.; Duan, X.-M. *J. Phys. Chem. C* **2012**, *116*, 24930.
(15) Lang, S. M.; Bernhardt, T. M. *Phys. Chem. Chem. Phys.* **2012**, *14*, 9255.
(16) Yang, X.-F.; Wang, A.; Qiao, B.; Li, J.; Liu, J.; Zhang, T. *Acc. Chem. Res.* **2013**, *46*, 1740.
(17) Lei, Y.; Mehmood, F.; Lee, S.; Greeley, J.; Lee, B.; Seifert, S.; Winans, R. E.; Elam, J. W.; Meyer, R. J.; Redfern, P. C.; Teschner, D.; Schlogl, R.; Pellin, M. J.; Curtiss, L. A.; Vajda, S. *Science* **2010**, *328*, 224.
(18) Liu, C.; Yang, B.; Tyo, E.; Seifert, S.; DeBartolo, J.; von Issendorff, B.; Zapol, P.; Vajda, S.; Curtiss, L. A. *J. Am. Chem. Soc.* **2015**, *137*, 8676.
(19) Li, F.; Li, Y.; Zeng, X. C.; Chen, Z. *ACS Catal.* **2015**, *5*, 544.
(20) Lin, J.; Wang, A.; Qiao, B.; Liu, X.; Yang, X.; Wang, X.; Liang, J.; Li, J.; Liu, J.; Zhang, T. *J. Am. Chem. Soc.* **2013**, *135*, 15314.
(21) Qiao, B.; Wang, A.; Yang, X.; Allard, L. F.; Jiang, Z.; Cui, Y.; Liu, J.; Li, J.; Zhang, T. *Nat. Chem.* **2011**, *3*, 634.
(22) Huang, Z.; Gu, X.; Cao, Q.; Hu, P.; Hao, J.; Li, J.; Tang, X. *Angew. Chem., Int. Ed.* **2012**, *51*, 4198.
(23) Wang, L.; Zhang, S.; Zhu, Y.; Patlolla, A.; Shan, J.; Yoshida, H.; Takeda, S.; Frenkel, A. I.; Tao, F. *ACS Catal.* **2013**, *3*, 1011.
(24) Deng, H.; Yu, Y.; He, H. *J. Phys. Chem. C* **2015**, *119*, 3132.
(25) Kwak, J. H.; Hu, J.; Mei, D.; Yi, C.-W.; Kim, D. H.; Peden, C. H.; Allard, L. F.; Szanyi, J. *Science* **2009**, *325*, 1670.
(26) Herzing, A. A.; Kiely, C. J.; Carley, A. F.; Landon, P.; Hutchings, G. J. *Science* **2008**, *321*, 1331.
(27) Zheng, Y.; Jiao, Y.; Zhu, Y.; Li, L. H.; Han, Y.; Chen, Y.; Du, A.; Jaroniec, M.; Qiao, S. Z. *Nat. Commun.* **2014**, *5*, 3783.
(28) Gao, G.; Jiao, Y.; Ma, F.; Jiao, Y.; Waclawik, E.; Du, A. *J. Catal.* **2015**, *332*, 149.
(29) Liu, J.; Liu, Y.; Liu, N.; Han, Y.; Zhang, X.; Huang, H.; Lifshitz, Y.; Lee, S.-T.; Zhong, J.; Kang, Z. *Science* **2015**, *347*, 970.
(30) Ma, X.; Lv, Y.; Xu, J.; Liu, Y.; Zhang, R.; Zhu, Y. *J. Phys. Chem. C* **2012**, *116*, 23485.
(31) Gao, G.; Jiao, Y.; Ma, F.; Jiao, Y.; Waclawik, E.; Du, A. *Phys. Chem. Chem. Phys.* **2015**, *17*, 31140.
(32) Maeda, K.; Wang, X.; Nishihara, Y.; Lu, D.; Antonietti, M.; Domen, K. *J. Phys. Chem. C* **2009**, *113*, 4940.
(33) Vilé, G.; Albani, D.; Nachtegaal, M.; Chen, Z.; Dontsova, D.; Antonietti, M.; López, N.; Pérez-Ramírez, J. *Angew. Chem., Int. Ed.* **2015**, *54*, 11265.
(34) Li, X.; Bi, W.; Zhang, L.; Tao, S.; Chu, W.; Zhang, Q.; Luo, Y.; Wu, C.; Xie, Y. *Adv. Mater.* **2016**, *28*, 2427.
(35) Kresse, G.; Furthmüller, J. *Comput. Mater. Sci.* **1996**, *6*, 15.
(36) Kresse, G.; Furthmüller, J. *Phys. Rev. B: Condens. Matter Mater. Phys.* **1996**, *54*, 11169.
(37) Perdew, J. P.; Burke, K.; Ernzerhof, M. *Phys. Rev. Lett.* **1996**, *77*, 3865.
(38) Perdew, J. P.; Ernzerhof, M.; Burke, K. *J. Chem. Phys.* **1996**, *105*, 9982.
(39) Grimme, S. *J. Comput. Chem.* **2006**, *27*, 1787.
(40) Henkelman, G.; Uberuaga, B. P.; Jónsson, H. *J. Chem. Phys.* **2000**, *113*, 9901.

(41) Heyd, J.; Scuseria, G. E.; Ernzerhof, M. *J. Chem. Phys.* **2003**, *118*, 8207.

(42) Heyd, J.; Scuseria, G. E.; Ernzerhof, M. *J. Chem. Phys.* **2006**, *124*, 219906.

(43) Gajdoš, M.; Hummer, K.; Kresse, G.; Furthmüller, J.; Bechstedt, F. *Phys. Rev. B: Condens. Matter Mater. Phys.* **2006**, *73*, 045112.

(44) Shi, H.; Chen, G.; Zhang, C.; Zou, Z. *ACS Catal.* **2014**, *4*, 3637.

(45) Wang, X.; Maeda, K.; Thomas, A.; Takanabe, K.; Xin, G.; Carlsson, J. M.; Domen, K.; Antonietti, M. *Nat. Mater.* **2009**, *8*, 76.

(46) *CRC Handbook of Chemistry and Physics*; Haynes, W. M., Ed.; CRC Press: Boca Raton, FL, 2014.